

# EXTINCTION IN THE LARGE MAGELLANIC CLOUD BAR AROUND NGC 1854, NGC 1856, AND NGC 1858

GUIDO DE MARCHI

European Space Research and Technology Centre, Keplerlaan 1, 2200 AG Noordwijk, Netherlands; gdemarchi@esa.int

NINO PANAGIA

Space Telescope Science Institute, 3700 San Martin Drive, Baltimore MD 21218, USA; panagia@stsci.edu and  
Supernova Limited, OYV #131, Northsound Rd., Virgin Gorda, British Virgin Islands

ANTONINO P. MILONE

Dipartimento di Fisica e Astronomia, Univ. di Padova, Vicolo dell'Osservatorio 3, Padova I-35122, Italy; antonino.milone@unipd.it and  
Istituto Nazionale di Astrofisica – Osservatorio Astronomico di Padova, Vicolo dell'Osservatorio 5, Padova I-35122, Italy

(Received 10 July 2021; Accepted 23 September 2021)

*Draft version September 29, 2021*

## ABSTRACT

We report on the extinction properties in the fields around the clusters NGC 1854, NGC 1856, and NGC 1858 in the bar of the Large Magellanic Cloud (LMC). The colour–magnitude diagrams of the stars in all these regions show an elongated red giant clump (RC) that reveals a variable amount of extinction across these fields, ranging from  $A_V \simeq 0.2$  to  $A_V \simeq 1.9$ , including Galactic foreground extinction. The extinction properties nonetheless are remarkably uniform. The slope of the reddening vectors measured in the  $(V-I, V)$  and  $(B-I, B)$  colour–magnitude planes is fully in line with the  $A_V/E(B-V) \simeq 5.5$  value found in the outskirts of 30 Dor. This indicates the presence of an additional grey extinction component in the optical requiring big grains to be about twice as abundant as in the diffuse Galactic interstellar medium (ISM). Areas of higher extinction appear to be systematically associated with regions of more intense star formation, as measured by the larger number of stars more massive than  $8 M_\odot$ , thus making injection of big grains into the ISM by SNII explosion the likely mechanism at the origin of the observed grey extinction component.

**Keywords:** dust, extinction — stars: formation — galaxies: stellar content - galaxies: Magellanic Clouds  
- galaxies: star clusters — open clusters and associations: individual (NGC1854, NGC1856, NGC1858)

## 1. INTRODUCTION

An investigation of the extinction properties towards a number of regions of recent star formation in the Large Magellanic Cloud (De Marchi & Panagia 2014, 2019; De Marchi et al. 2014, 2016, 2020) has so far revealed a consistent picture: shortwards of  $\sim 1 \mu\text{m}$ , the extinction curve is systematically flatter (in logarithmic units) than in the diffuse interstellar medium (ISM). This points to the presence of a grey component due to a larger proportion of big grains. In the regions studied so far (30 Dor, NGC 2060, NGC 1938), the total extinction is not only uneven, but also rather large for the LMC, with  $A_V \lesssim 2$ .

We have undertaken a systematic study of all the LMC star-forming regions for which high-quality photometry with the *Hubble Space Telescope* (HST) is available, in an attempt to understand whether and how the extinction properties depend on the actual amount of extinction present in these fields. In the Milky Way, regions of heavy extinction along the Galactic plane have long been known to show a ratio of total-to-selective extinction  $R_V \equiv A_V/E(B-V)$  systematically larger than the value of  $\sim 3.1$  typical of the diffuse ISM. Examples include the Orion Nebula, NGC 2244, I Ara, IC 2851 (see, e.g., Sharpless 1952; Sharpless 1962; Johnson 1965; Turner 1973; Herbst 1975). In this work we consider three additional LMC clusters located in the bar of the galaxy, which are subject to intermediate values of  $A_V$ , in order to explore whether the extinction properties and the value of  $R_V$  depend indeed on the amount of dust in these fields.

The first is the cluster NGC 1858. The only study so far of the stellar populations in this cluster based on digital photometry is that of Vallenari et al. (1994). Adopting  $E(B-V) = 0.15 \pm 0.05$  (from Caplan & Deharveng 1984), these authors show that the most likely age of the main cluster population is 8–10 Myr, although the presence of a protostar in the field (Epchtein et al. 1984) suggests that some star formation might still be active.

The second is the cluster NGC 1854 (also called NGC 1855). In a study based on photoelectric photometry, Connolly & Tifft (1977) showed that the cluster has a tight main sequence (MS) and derived an age of  $25 \pm 15$  Myr, with a colour excess  $E(B-V)$  about 0.1 mag redder than the neighbouring field. The age determination is fully consistent with later works based on photographic photometry by Hodge (1983), suggesting  $30 \pm 10$  Myr, and by Alcaïno & Liller (1987), who derived  $25 \pm 6$  Myr. No results based on digital photometry exist in the literature for this cluster.

The third cluster is NGC 1856, whose stellar population and extended MS turn-off in the colour-magnitude diagram (CMD) have been extensively studied in the past decade. Works by Bastian & Silva-Villa (2013), D’Antona et al. (2015), Correnti et al. (2015), and Milone et al. (2015) concur in assigning to it an age of  $\sim 300$  Myr. Correnti et al. (2015) and Milone et al. (2015) address the presence of uneven extinction across the cluster. They assume that the extinction properties, namely the extinction law and direction of the reddening vector, are those of the “standard” MW ex-

tion curve. In this work we will not cover the NGC 1856 cluster itself, but rather four regions adjacent to it, at a projected distance of  $\sim 5'$  or  $\sim 75$  pc, specifically to probe an area still relatively close to NGC 1854 and NGC 1858 (about 200 pc to the south) but not affected by recent massive star formation episodes.

In this paper, we investigate the origin of the patchy extinction causing differential reddening across the fields around NGC 1854, NGC 1856, and NGC 1858 and show that the extinction properties, and the grain size distribution that they imply, are consistent with those measured in a field North of NGC 2060. The structure of the paper is as follows. In Section 2 we present the observations and their analysis. In Section 3 we discuss the different populations present in the fields, while Section 4 is devoted to the extinction properties, which we compare with those of other regions in the LMC. A discussion and the conclusions follow, respectively, in Sections 5 and 6.

## 2. OBSERVATIONS AND DATA ANALYSIS

The fields around the clusters NGC 1854, NGC 1856, and NGC 1858 were observed with the *Wide Field Channel* (WFC) of the *Advanced Camera for Surveys* (ACS) on board the HST. Colour composite images of the regions studied in this work are shown in Figure 1, while details on the filters, exposure times, and dates of the observations are contained in Table 1.

The effective point spread function (ePSF) fitting procedure developed by Anderson et al. (2008) was used for the astrometric and photometric analysis of the images. The stellar positions derived in this way were further corrected for geometric distortion by using the solution by Anderson & King (2006). The instrumental magnitudes were calibrated in the VEGAMAG reference system following Anderson et al. (2008), with the zero-point values taken from the ACS Zeropoints Calculator (see Ryon 2019). Throughout this paper we will refer to the magnitudes in the F475W, F555W, and F814W bands as, respectively,  $B$ ,  $V$ , and  $I$ .

Even with the shortest amongst the exposures times listed in Table 1, some non linearity and saturation of the detector's response is unavoidable for the brightest stars. In the NGC 1854 field, stars brighter than  $V = 16.2$  and  $I = 15.8$  are saturated. For NGC 1858 saturation occurs for stars with  $V \leq 15.2$  and  $I \leq 15.0$ , while in the fields around NGC 1856 this happens for stars with  $B \leq 19.3$  and  $I \leq 15.7$ . Nevertheless, the intrinsic brightness of these stars was fully recovered by summing over pixels into which bleeding occurred as a result of the over-saturation (see Gilliland 2004 and Anderson et al. 2008 for details).

Photometric uncertainties on the magnitudes and colours of non-saturated stars are very small (see Table 2). The magnitudes of stars within about 2 mag of the saturation limit are recovered with an accuracy of typically 0.02–0.03 mag.

In our analysis we considered only stars with small root-mean-square scatter in position measurements and well fitted by the ePFS routine (Anderson et al. 2008). This sample of stars with “high quality” photometry was selected as in Milone et al. (2009, see their Figure 1) on the basis of the various diagnostics of the astrometric and photometric quality provided by the computer programmes by Anderson et al. (2008).

**Table 1**  
Observations used in the paper.

| Cluster     | Filter | Exposure time  | Date        | Proposal |
|-------------|--------|----------------|-------------|----------|
| NGC 1854    | F555W  | 50             | 2003 Oct 07 | 9891     |
|             | F814W  | 40             | 2003 Oct 07 | 9891     |
| NGC 1858    | F555W  | 20             | 2003 Oct 08 | 9891     |
|             | F814W  | 20             | 2003 Oct 08 | 9891     |
| NGC 1856 F1 | F475W  | $2 \times 665$ | 2014 Feb 09 | 13379    |
|             | F814W  | $42 + 559$     | 2014 Feb 09 | 13379    |
| NGC 1856 F2 | F475W  | $2 \times 665$ | 2014 Mar 24 | 13379    |
|             | F814W  | $42 + 559$     | 2014 Mar 24 | 13379    |
| NGC 1856 F3 | F475W  | $2 \times 665$ | 2014 May 18 | 13379    |
|             | F814W  | $42 + 559$     | 2014 May 18 | 13379    |
| NGC 1856 F4 | F475W  | $2 \times 665$ | 2014 Jun 06 | 13379    |
|             | F814W  | $42 + 559$     | 2014 Jun 06 | 13379    |

**Note.** — Exposure times are in seconds.

**Table 2**  
Photometric uncertainties.

| Magnitude | NGC 1854   |                | NGC 1856   |                | NGC 1858   |                |
|-----------|------------|----------------|------------|----------------|------------|----------------|
|           | $\sigma_V$ | $\sigma_{V-I}$ | $\sigma_B$ | $\sigma_{B-I}$ | $\sigma_V$ | $\sigma_{V-I}$ |
| 15.00     | 0.016      | 0.022          | —          | —              | 0.014      | 0.019          |
| 15.50     | 0.015      | 0.020          | —          | —              | 0.013      | 0.017          |
| 16.00     | 0.014      | 0.019          | —          | —              | 0.013      | 0.018          |
| 16.50     | 0.013      | 0.018          | —          | —              | 0.012      | 0.019          |
| 17.00     | 0.013      | 0.017          | —          | —              | 0.015      | 0.021          |
| 17.50     | 0.012      | 0.019          | —          | —              | 0.015      | 0.022          |
| 18.00     | 0.015      | 0.021          | —          | —              | 0.017      | 0.025          |
| 18.50     | 0.015      | 0.022          | —          | —              | 0.022      | 0.032          |
| 19.00     | 0.017      | 0.027          | —          | —              | 0.025      | 0.036          |
| 19.50     | 0.022      | 0.033          | 0.013      | 0.018          | 0.030      | 0.044          |
| 20.00     | 0.025      | 0.038          | 0.012      | 0.017          | 0.037      | 0.053          |
| 20.50     | 0.030      | 0.046          | 0.012      | 0.019          | 0.043      | 0.062          |
| 21.00     | 0.037      | 0.054          | 0.014      | 0.021          | 0.056      | 0.078          |
| 21.50     | 0.044      | 0.062          | 0.015      | 0.022          | 0.073      | 0.097          |
| 22.00     | 0.057      | 0.076          | 0.016      | 0.023          | 0.086      | 0.115          |
| 22.50     | 0.073      | 0.097          | 0.020      | 0.028          | 0.097      | 0.130          |
| 23.00     | —          | —              | 0.024      | 0.033          | —          | —              |
| 23.50     | —          | —              | 0.028      | 0.038          | —          | —              |
| 24.00     | —          | —              | 0.035      | 0.046          | —          | —              |
| 24.50     | —          | —              | 0.041      | 0.055          | —          | —              |
| 25.00     | —          | —              | 0.052      | 0.067          | —          | —              |

**Note.** — Values for NGC 1856 are representative of all fields F1–F4.

## 3. COLOUR–MAGNITUDE DIAGRAMS: MULTIPLE POPULATIONS

We show in Figures 2 and 3 the CMDs obtained from the stars with high-quality photometry in the fields including and surrounding NGC 1858 and NGC 1854, respectively. The CMDs reveal a complex population, made up of stars in different evolutionary phases. In Panel a) of both figures small grey dots sample a region of 12.5 pc radius around the nominal centres of the two clusters (dashed circles in Figure 1). Objects within the inner 6.5 pc are indicated with thick black dots. Both regions reveal a young population of stars in the upper main sequence (MS) and a sparsely populated red giant branch (RGB). Also shown are theoretical isochrones from the models of Chen et al. (2015) for metallicity  $Z = 0.007$ , since this is a typical value for the LMC (e.g., Hill et al. 1995; Geha et al. 1998). All isochrones already include a distance modulus  $(m-M)_0 = 18.55$  (Panagia 1998) for the LMC and the reddening contribution of the Milky Way along the line of sight to these clusters, namely  $A_V = 0.22$  (e.g., Fitzpatrick & Savage 1984), which corresponds to  $E(B-V) = 0.07$  and  $E(V-I) = 0.11$  for the extinction law of the diffuse Galactic ISM (e.g., Cardelli et al. 1989; Fitzpatrick & Massa 1990).

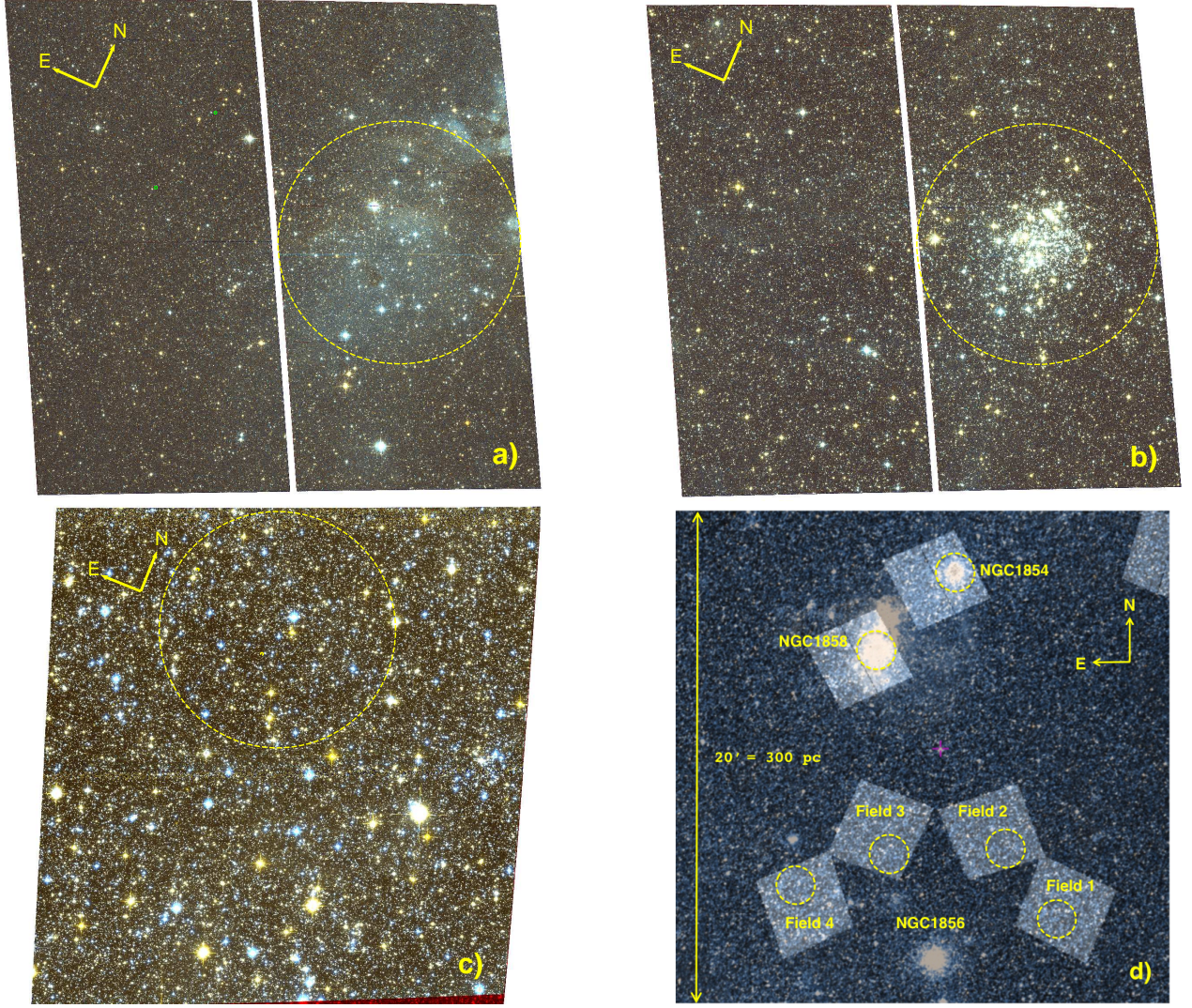


**Figure 1.** Colour composite images of the regions studied in this work. Panel a) and b), corresponding respectively to fields around NGC 1858 and NGC 1854, were obtained by combining the exposures in the  $V$  and  $I$  bands. Panel c) corresponds to Field 4, located to the north-east of NGC 1856, and was obtained from the combination of the  $B$  and  $I$  bands. The three fields span approximately  $205''$  or  $\sim 50$  pc on a side. Panel d) shows the projected distribution of the fields on the plane of the sky, in a region of about  $20'$  or  $\sim 300$  pc on a side. The yellow circles, with a radius of  $50''$  of 12.5 pc, indicate the areas corresponding to the CMDs shown in Figures 2 – 4.

The best fit to the upper MS of NGC 1858 is obtained for an age of 5 Myr (blue solid line in Figure 2a) and requires an extra  $E(V-I) = 0.08$  component of color excess in addition to the foreground  $E(V-I) = 0.11$  mentioned above,<sup>1</sup> thus in total  $E(V-I) = 0.19$ . With the same total reddening, the blue supergiant HD 261196 at  $V = 12.07$ ,  $V-I = 0.20$  is compatible with an age of  $\sim 13$  Myr (red dashed line). We note that for this object we have used the magnitudes published by Bonanos et al. (2009) because in our ACS images the star is saturated.

Concerning NGC 1854, the best fit to its upper MS is also obtained for an age of 5 Myr (blue solid line in Figure 3a) and a slightly larger value of the colour excess, namely  $E(V-I) = 0.21$ . Adopting the same extinction value also for the supergiants located near  $V = 14$ ,  $V-I = 0.3$  suggests an age around 60 Myr for these objects (red dashed line).

The CMDs of both clusters (Figures 2a and 3a) also reveal a sparsely populated RGB, which however is consistent with

contamination by LMC field stars along the line of sight falling within the selected radius. To explore this, we counted the number of stars inside the dashed areas of the CMDs in Figures 2a and 3a and compared them with the number of objects in identical regions of the CMDs of the comparison fields. The latter are shown in Figures 2b and 3b, and include all stars farther than 12.5 pc from the centres of NGC 1858 and NGC 1854, respectively. Once scaled by the relative areas spanned by each cluster and its comparison field, the number of stars within the dashed trapezoids in the CMDs of the cluster and of the field are indistinguishable, within statistical uncertainties.

Furthermore, objects in the RGB phase would not be compatible with the young ages of both clusters, in the range 5 – 60 Myr derived above, requiring instead ages in excess of  $\sim 1$  Gyr. This is shown graphically in Figures 2b and 3b, where over the CMDs of the comparison fields surrounding NGC 1858 and NGC 1854 we show theoretical isochrones for ages of 1.5, 2, 3, and 4 Gyr, respectively in green, red, orange, and blue. The isochrones are taken from the models of Tang

<sup>1</sup> As we will show in Section 5, in all these regions also the ratio  $R_V$  between total and selective extinction is considerably higher than the characteristic  $R_V = 3.1$  value typical of the diffuse Galactic ISM.

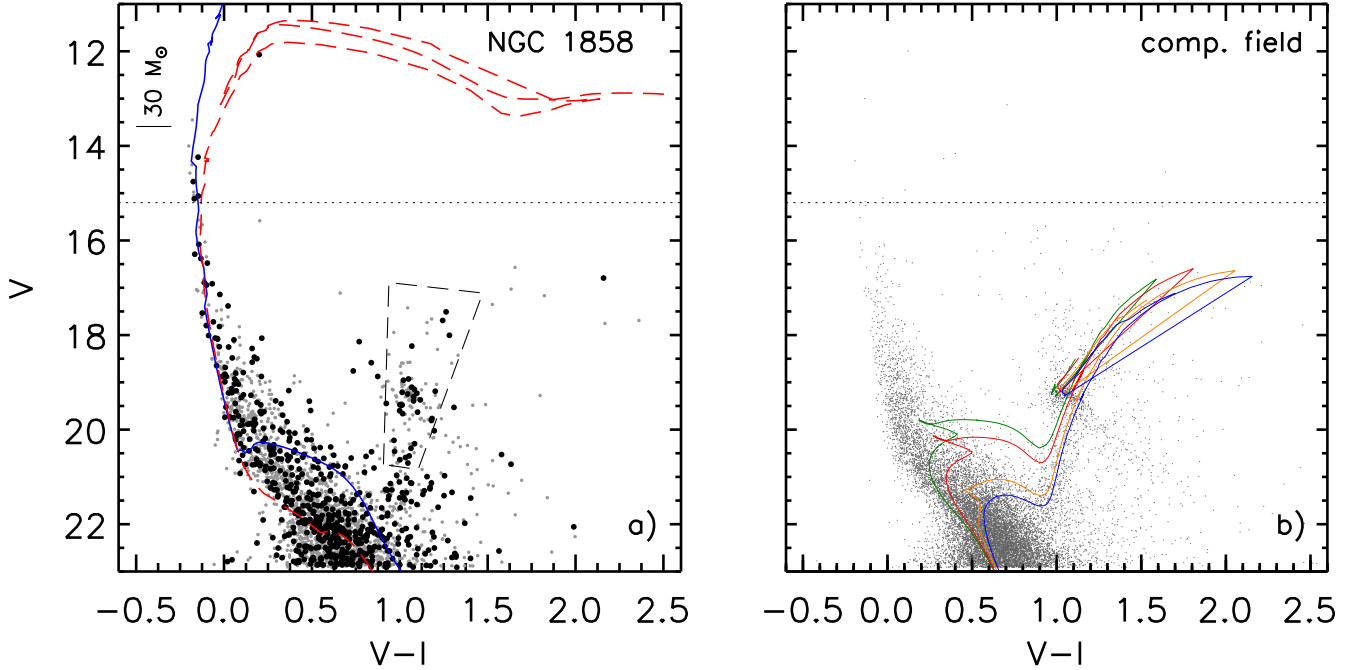


**Figure 2.** CMDs of high-quality stars in and around NGC 1858. In Panel a), small grey dots are used for stars within a radius of 12.5 pc of the nominal centre (see Figure 1), while thick black dots mark objects within 6.25 pc of it. The solid and dashed lines show isochrones from the models of Chen et al. (2015) for ages of 5 and 18 Myr, respectively, for the appropriate LMC distance, metallicity  $Z = 0.007$ , and a combined colour excess (foreground + intrinsic) of  $E(V-I) = 0.19$ . We also indicate the approximate mass of the heaviest stars consistent with the youngest isochrone. The CMD in Panel b) is obtained from all stars more distant than 12.5 pc from the centre of NGC 1858 and the theoretical isochrones are from the models of Tang et al. (2014) for metallicity  $Z = 0.004$  and only Galactic foreground extinction of  $E(V-I) = 0.11$ . Ages of 1.5, 2, 3, and 4 Gyr are shown, respectively, in green, red, orange, and blue. In all panels the thin horizontal lines indicate the saturation level discussed in Section 2.

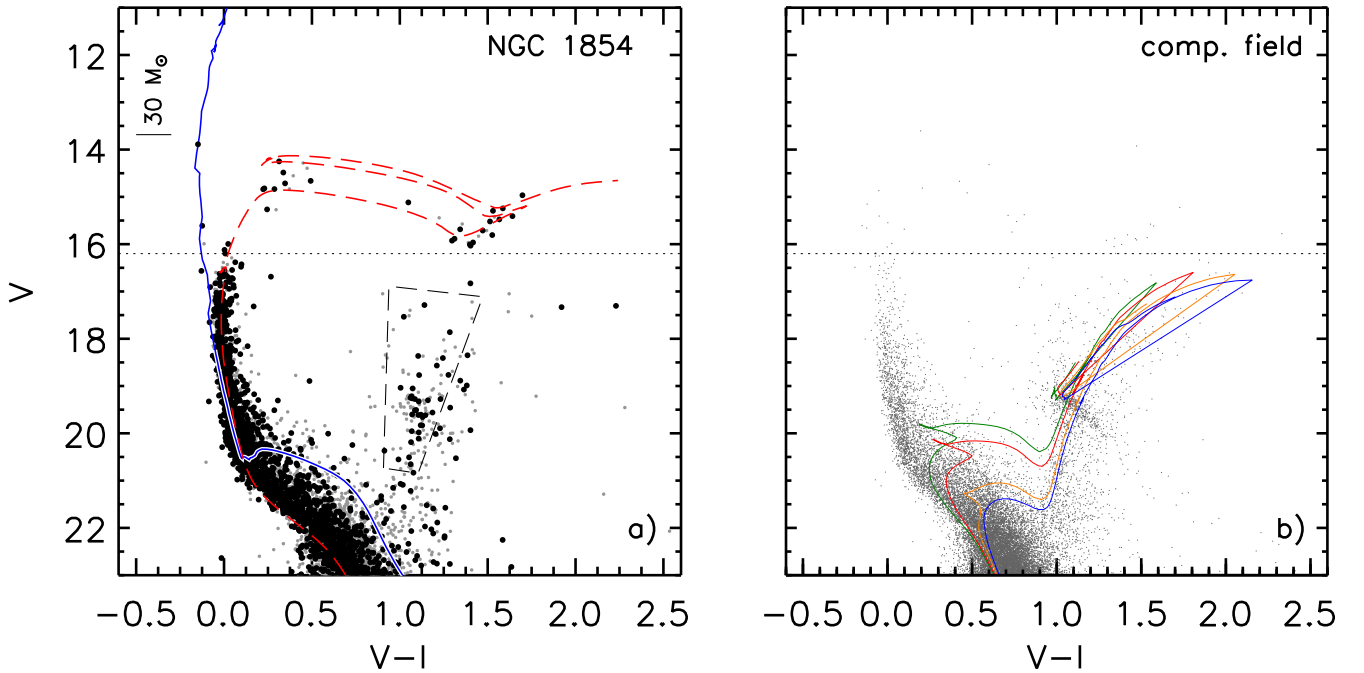


**Figure 3.** Same as Figure 2 but for stars in and around NGC 1854. The only difference is in Panel a), where the combined colour excess (foreground + intrinsic) applied to the isochrones is  $E(V-I) = 0.21$  and the ages of the isochrones are 5 (solid line) and 60 Myr (dashed line).

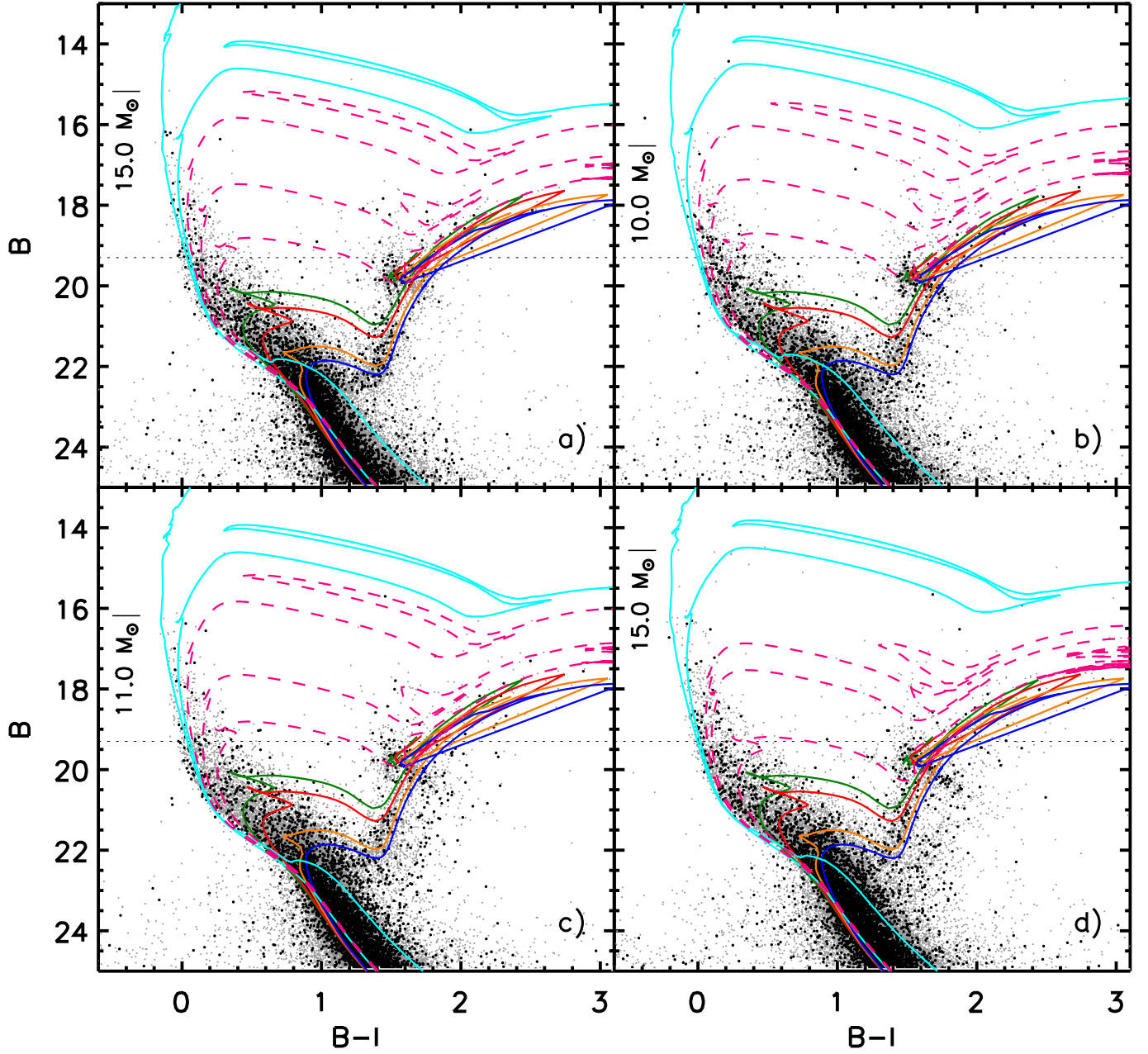


**Figure 4.** CMDs of the four regions around NGC 1856 indicated in Figure 1. Small grey dots mark all stars, while thick black dots indicate objects within the circles shown in Figure 1 (radius 12.5 pc, for ease of comparison with Figures 2 and 3). Isochrones from Tang et al. (2014) for metallicity  $Z = 0.004$  and ages of 1.5, 2, 3, and 4 Gyr (shown respectively, by green, red, orange, and blue thin solid lines) are the same in all panels and only include foreground Galactic extinction  $A_V = 0.22$ , corresponding  $E(B-I) = 0.18$  for the Galactic extinction law (same as in Figures 2b and 3b). Isochrones for younger ages are from the models of Chen et al. (2015) for metallicity  $Z = 0.007$  and ages and colour excess as follows. In Panel a), from Region 1, the thick solid (cyan) lines correspond to ages of 10 and 50 Myr and a combined colour excess (foreground + intrinsic)  $E(B-I) = 0.33$ , while the dashed lines represent ages of 100, 270, and 600 Myr with the same combined colour excess. In Panel b), corresponding to Region 2, the ages are of 10 and 50 Myr for the thick solid lines (cyan), while the dashed lines represent ages of 120, 270, and 600 Myr, with a combined colour excess  $E(B-I) = 0.28$ . In Panel c), from Region 3, the thick solid (cyan) lines are for ages of 12 and 60 Myr, while the thick dashed lines are for ages of 100, 300, and 600 Myr, all of them with combined colour excess  $E(B-I) = 0.32$ . In panel d), from Region 4, the thick solid (cyan) lines are for ages of 12 and 50 Myr, and the thick dashed lines for ages of 200, 300, and 800 Myr, again with combined colour excess  $E(B-I) = 0.28$ .

et al. (2014) for metallicity  $Z = 0.004$  and already include Galactic foreground extinction of  $E(V-I) = 0.11$ . We do not include any additional colour excess with these isochrones since old LMC field stars can be located anywhere along the line of sight, not only behind but also in front of the young clusters, whose exact position is not known. We also note that, in principle, red clump stars in this field could have ages up to 10 Gyr. However, as Girardi & Salaris (2000) pointed out, the age distribution of red clump stars in galaxies with constant star formation is strongly skewed towards younger ages, due to the longer lifetimes of more massive RC stars and to the decreasing rate at which stars leave the MS at older ages. Moreover, as pointed out in De Marchi et al. (2014), RC stars with ages between 3 and 9 Gyr change very little their intrinsic positions in the CMDs. This justifies limiting our interval of ages up to  $\sim 4$  Gyr.

Besides a broad MS, the prominent RGB is the characteristic feature of these CMDs, together with a remarkably elongated RC, extending by over one magnitude in  $V$  and suggesting a considerable amount of differential reddening in these fields. The extended RC is clearly not caused by age effects, since all isochrones agree with the overdensity observed in the CMD at  $V-I \simeq 1.0$ ,  $V \simeq 19.2$  (the nominal RC location), but not with the extended tail. More details on the effects of a range of ages on the shape and extent of the RC in the CMD are provided by De Marchi et al. (2014). In particular, for the metallicity  $Z = 0.004$  that is relevant to this work, their Figure 4 shows that the combination of stellar populations with ages ranging from 1.4 to 3 Gyr only causes a broadening of less than 0.05 and 0.02 mag ( $1\sigma$ ) respectively on the  $V$  magnitude and  $B-V$  colour of the resulting RC ( $\sigma = 0.02$  mag is also the value found in the  $V-I$  colour). Considering that the nominal RC position corresponding to each individual age already has an intrinsic spread of  $\sim 0.1$  mag in  $V$  and  $\sim 0.05$  mag in  $B-V$ , the broadening introduced by the age spread is marginal.

The CMDs of the third region studied in this work, around NGC 1856, are shown in Figure 4. As mentioned in Section 2, we selected observations of four fields surrounding (but not containing) the cluster, at a typical distance of  $5'$  or about 75 pc from the cluster centre (see Figure 1). In these regions no concentrations of objects or clustering of bright stars are seen, indicating that these areas are dominated by LMC field stars. In Figure 4 we show the CMDs of the four fields, using small grey dots to indicate all objects and thick black dots for stars within the circular regions shown in Figure 1. The circular regions, with a radius of 12.5 pc, have been selected to simplify the comparison with the CMDs of the fields around NGC 1858 and NGC 1854, but they do not correspond to any overdensity of objects, as mentioned above.

Most stars in these fields are old, as indicated by the prominent RGB, for which comparison with isochrones suggests ages older than  $\sim 1$  Gyr. The green, red, orange, and blue isochrones are the same as shown in Figures 2b and 3b from Tang et al. (2014) for ages of 1.5, 2, 3 and 4 Gyr, metallicity  $Z = 0.004$ , and already include Galactic foreground extinction, which in these bands amounts to  $E(B-I) = 0.18$ .

Besides old stars, a much younger population is also present in these CMDs, as witnessed by the many upper MS stars. These objects are compatible with ages in the range  $\sim 10-50$  Myr (for details see caption to Figure 4) and masses up to  $\sim 10-15 M_{\odot}$ . Furthermore, a number of objects in the range  $0.6 \lesssim B-I \lesssim 1.6$  and  $16 \lesssim B \lesssim 19$  are consistent with giants with ages in the range  $\sim 100-600$  Myr. Thus, in spite of

the lack of clear clustering or overdensities, in these regions star formation has been proceeding in the past several 10 Myr and in the past several 100 Myr. This finding will be crucial for understanding the extinction properties in these fields (see Section 5).

Like in the case of the fields around NGC 1858 and NGC 1854, also here does the RC show an extended shape, suggesting the presence of patchy extinction. The extent of the RC elongation is not the same in all fields and increases proceeding from Panel a) to d). In the following section we will study the extinction properties in all these fields through an analysis of the shape of the extended RC.

#### 4. RED CLUMP STARS TO PROBE EXTINCTION

The stability associated with the phase of central He-burning characteristic of RC stars (e.g. Cannon 1970) makes these objects excellent tracers of reddening, when the distance is known. Girardi & Salaris (2001) and Salaris & Girardi (2002) presented a detailed study of the properties of the mean RC as a function of age, metallicity, and star-formation history. As shown in Figures 2, 3, and 4, the expected location of the RC in the CMD is only marginally affected by age differences as large as 2.5 Gyr. To be sure, when objects with different ages and metallicities are present in the stellar population, the RC does take on a slightly elongated shape, but De Marchi et al. (2014) showed that for LMC stars these effects account for a dispersion of at most 0.2 mag in the  $V$  and  $I$  bands when both the age and metallicity vary by a factor of two.

Also considerable dispersion in distance along the line of sight could of course cause the RC to appear elongated in the CMD, albeit only vertically, along the magnitude axis, since distance does not have any effect on the colour of stars. Moreover, for stars in the LMC this effect is negligible, since that galaxy is seen at a high inclination ( $\sim 35^\circ$ ) and its disc has a scale height of typically less than 0.5 kpc (Van der Marel & Cioni 2001), which is not significant when compared with the distance to the LMC itself ( $51.4 \pm 1.2$  kpc; Panagia et al. 1991, and updates in Panagia 1998, 1999). Indeed, an exponential distribution with a scale height of 0.5 kpc at the distance of the LMC results in a median deviation along the line of sight of less than 0.02 mag even including the thickening caused by the  $35^\circ$  inclination. For 83 % of the stars the deviation is less than 0.05 mag. The effect of distance along the line of sight is, therefore, negligible. Even when combined with the small broadening of the RC caused by age differences, these effects remain barely detectable and cannot account for the substantial RC elongation in colour and magnitude that we observe in these regions.

In this work we are interested not only in the elongation of the RC, which is a measure of the total extinction in the field, but also in the slope of the extended RC in the CMD, since this gives a fully empirical measure of the direction of the reddening vector (Nataf et al. 2013; De Marchi et al. 2014). Together, the two quantities provide information on the extinction properties in the field.

A practical method to measure both the length and the slope of the RC feature in the CMD is to apply the unsharp-masking technique. De Marchi et al. (2016) provide a detailed description of the method, which we briefly summarise here. The purpose of unsharp masking is to make an image of the CMD

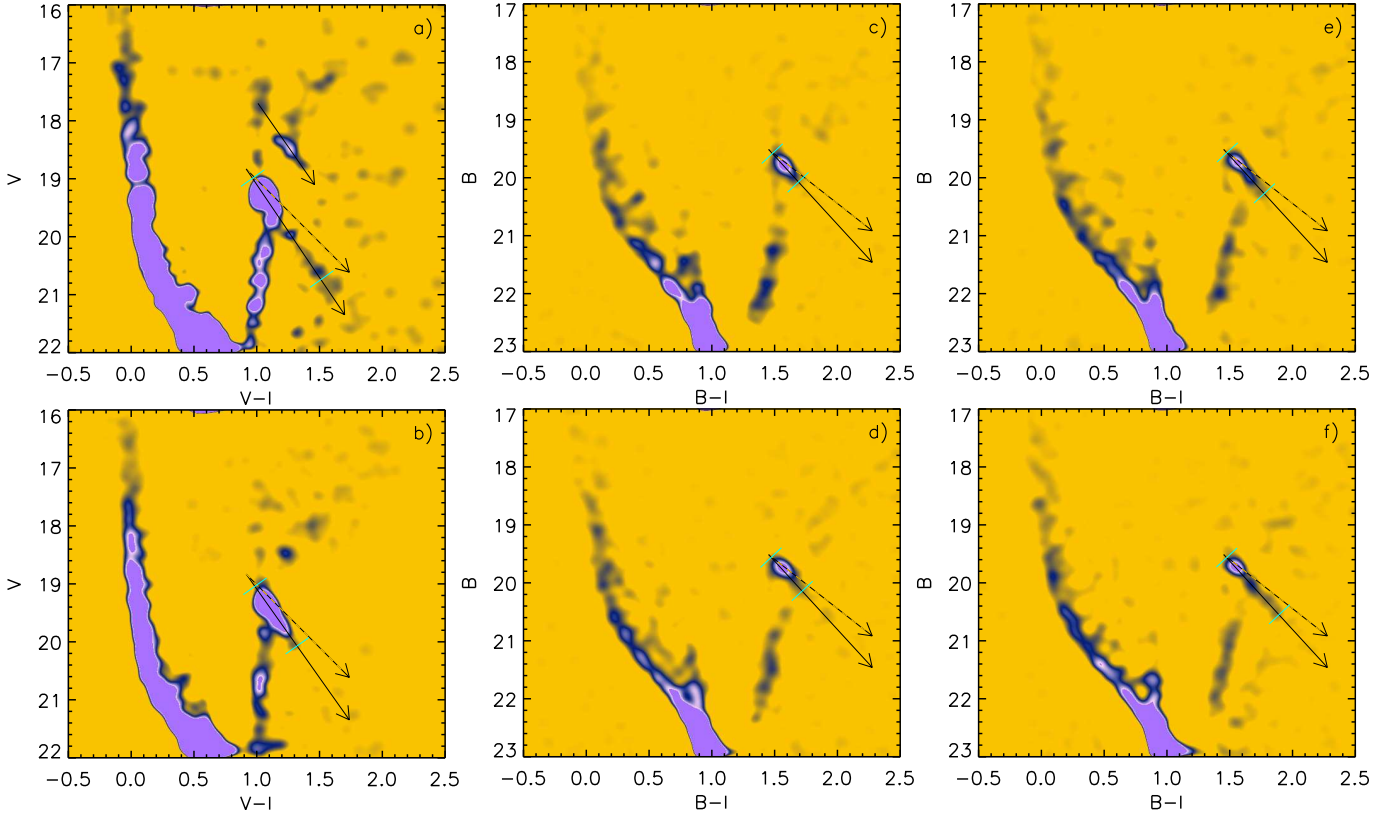


**Figure 5.** Unsharp masking applied to all CMDs. Panels are as follows: a) NGC 1858; b) NGC 1854; c) NGC 1856 F1; d) NGC 1856 F2; e) NGC 1856 F3; f) NGC 1856 F4. The slope of the reddening vector is obtained through a linear fit to the elongated RC. The extent of the elongated RC is indicated by the tick marks. The short solid arrow starting at  $V \simeq 17.6$  in panel a) is parallel to the reddening vector for this field and provides a good fit to the younger extended RC.

sharper by subtracting from it a mask consisting of a blurred version of the CMD image itself. First, to obtain the image of the CMD, each object in it is mapped to a two-dimensional array, with a sampling of 0.01 mag in colour and magnitude. The array is then convolved with a narrow Gaussian beam, which assigns to each point in the CMD the resolution pertaining to the photometric uncertainties. We used a beam size  $\sigma = 0.08$  mag, corresponding to about three times the typical photometric uncertainty. Similarly, to obtain the blurred mask, the same array is convolved with a wider Gaussian beam, in our case  $\sigma = 0.3$  mag. The mask is then subtracted from the CMD image. Analytically, these operations are equivalent to convolving the CMD with a kernel represented by the difference between two Gaussian beams with different  $\sigma$  (see De Marchi et al. 2016). We experimented with different values for the wider Gaussian beam (namely 0.2 and 0.4 mag) and the differences are imperceptible.

We show in Figure 5 the CMDs of the various regions after unsharp masking. Panels a) and b) refer to the regions surrounding NGC 1858 and NGC 1854, respectively, while Panels c) through to f) refer to fields F1 to F4 around NGC 1856. The high-frequency substructures are easier to identify than in the original CMDs, in particular the MS, the MS turn-off, the RG branch, and of course the elongated RC. The direction of the reddening vector (thick solid arrows in Figure 5) is measured using the ridge line of the extended RC. The uncertainty on the slope is obtained using weights proportional to the local density of points in the CMD. In Figure 5, the dashed lines show the reddening vector corresponding to the extinction law of the Galactic diffuse ISM, in the bands specific to each panel. It is evident that in these regions the slope is considerably steeper than in the Galactic ISM, about 1.5 times as

steep.

The slope of the reddening vector corresponds in turn to the ratio between total ( $A$ ) and selective ( $E$ ) extinction in these specific bands. The values measured in the individual regions are given in Table 3, together with their uncertainties. We also show the values measured in the same bands in and around 30 Dor and in NGC 1938, together with their uncertainties, as well as the values corresponding to the average extinction law in the diffuse Galactic ISM. The uncertainty on the latter does not reflect the actual measurement errors, but rather the wide dispersion around the mean, exceeding 20% (see e.g. Herbst 1975; Massa et al. 1983; Fitzpatrick & Massa 2005; Nataf et al. 2016).

We note in passing that also the feature seen in Figure 5a at  $1.0 < V-I < 1.4$  and  $18.3 < V < 18.9$  is an elongated RC. Comparison with the Chen et al. (2015) isochrones mentioned above suggests that this RC is associated to a population of intermediate age,  $\sim 330$  Myr, and as such considerably younger than the population responsible for the main RC feature at fainter magnitudes. According to the isochrones, the unextinguished location of the RC for this population should be at  $V = 17.8$  and  $V-I = 1.0$ , where an enhancement is indeed present in the CMD, both before and after unsharp masking. The slope of the younger extended RC is consistent with the reddening vector measured elsewhere in this field (see short solid arrow). Its shape and appearance suggests that most of these RC stars are behind the NGC 1858 cluster, because of the gap that separates the nominal RC position at  $V = 17.8$  from the blue end of the elongation at  $V = 18.2$ . The implied minimum reddening value of  $A_V = 0.4$  is larger than the minimum intrinsic reddening revealed by the massive stars in the upper MS of NGC 1858, which is of the order of  $A_V = 0.25$

**Table 3**

Ratio of total and selective extinction in our regions. For comparison, we also indicate the values in the same bands in and around 30 Dor, as well as in the diffuse Galactic ISM.

| Region<br>(1)          | $A_V/E(V-I)$<br>(2) | $A_B/E(B-I)$<br>(3) |
|------------------------|---------------------|---------------------|
| NGC 1858               | $3.21 \pm 0.14$     |                     |
| NGC 1854               | $3.26 \pm 0.35$     |                     |
| NGC 1856 field 1       |                     | $2.70 \pm 0.53$     |
| NGC 1856 field 2       |                     | $2.31 \pm 0.26$     |
| NGC 1856 field 3       |                     | $2.29 \pm 0.28$     |
| NGC 1856 field 4       |                     | $2.33 \pm 0.12$     |
| NGC 1938               | $2.99 \pm 0.12$     |                     |
| 30 Dor                 | $2.97 \pm 0.08$     | $2.21 \pm 0.14$     |
| 30 Dor West (NGC 2060) | $3.17 \pm 0.29$     | $2.41 \pm 0.31$     |
| Diffuse Galactic ISM   | $2.17 \pm 0.44$     | $1.70 \pm 0.34$     |

(see Figure 2a).

## 5. DISCUSSION

Table 3 reveals that the reddening vectors for the lines of sight towards the three clusters and their surroundings are systematically steeper than those towards NGC 1938 or 30 Dor (where  $R_V = 4.5 \pm 0.2$ ; De Marchi & Panagia 2014). The slopes are more similar to those measured towards NGC 2060 (30 Dor West), where the extinction law derived by De Marchi et al. (2014) corresponds to  $R_V = 5.6 \pm 0.3$ . This suggests that the lines of sight towards NGC 1854, NGC 1856, and NGC 1858 share similar extinction properties to those towards 30 Dor West, with a value of  $R_V \simeq 5.5$ .

Similarly to 30 Dor and 30 Dor West, the likely reason for the elevated value of  $R_V$  in the direction of NGC 1854, NGC 1856, and NGC 1858 is the presence of a grey component, caused by an extra population of big grains, superposed to the more standard LMC extinction curve (Gordon et al. 2003). In 30 Dor, De Marchi & Panagia (2019) showed that the effect of the additional grey component is present at all wavelengths shorter than  $\sim 1 \mu\text{m}$  and through to the far ultraviolet range. That work reveals that the big grains responsible for the grey component towards 30 Dor are of the same nature as those present in the diffuse ISM of the MW, but their fraction is about twice as high. The higher value of  $R_V$  towards the three clusters studied here suggests possibly an even larger fraction of big grains.

We highlight that the extinction properties in these fields, as probed by the slope of the reddening vector, do not correlate with the amount of extinction, which is indicated by the length of the extended RC. All fields have a slope consistent with  $R_V \simeq 5.5$  but the range of extinction values across these fields varies considerably. This can be seen in Figure 5, where the extent of the RC in each CMD is marked by the short segments. The marks correspond to the farthest points along the RC where the density of stars exceeds the 95 percentile ( $2\sigma$ ) and provide a measure of the spread of extinction present in the fields. The bluest end of the RC corresponds to no intrinsic extinction (and hence with  $A_V \simeq 0.2$  once the Galactic foreground component is taken into account), while the most reddened end, towards NGC 1858, corresponds to  $A_V \simeq 1.7$  or total extinction  $A_V \simeq 1.9$  once also the contribution of the Milky Way is included.

The range of extinction values is derived from the magnitude difference between the marks, taking into account the intrinsic size of the undispersed RC, which in these bands amounts to  $\sim 0.1$  mag (Girardi & Salaris 2001). We under-

**Table 4**

Total extinction in each field, in various bands, compared with the number of stars more massive than  $8 M_\odot$ .

| Region<br>(1)    | $\Delta A_B$<br>(2) | $\Delta A_V$<br>(3) | $\Delta A_I$<br>(4) | $N$<br>(5) |
|------------------|---------------------|---------------------|---------------------|------------|
| NGC 1856 field 1 | 0.39                | <i>0.31</i>         | 0.18                | 6          |
| NGC 1856 field 2 | 0.48                | <i>0.38</i>         | 0.23                | 4          |
| NGC 1856 field 3 | 0.45                | <i>0.36</i>         | 0.22                | 4          |
| NGC 1856 field 4 | 0.88                | <i>0.72</i>         | 0.47                | 12         |
| NGC 1854         | <i>1.14</i>         | 0.93                | 0.59                | 11         |
| NGC 1858         | <i>1.94</i>         | 1.60                | 1.05                | 20         |

line that if instead of adopting  $\sigma = 0.3$  mag as the size of the smoothing Gaussian beam we had used 0.2 mag or 0.4 mag the resulting length of the RC would have been, respectively, 0.02 mag shorter or 0.01 mag longer than the  $A_V \simeq 1.9$  value given above. These differences are negligible when compared to the the intrinsic size of the undispersed RC.

As already mentioned in Section 4, De Marchi et al. (2014) showed that a spread of a factor of two on both the age and metallicity of the stars only broadens the size of the RC to about 0.2 mag in  $V$  and  $I$ . Because of the differential way in which they are derived, the measured extinction spreads are not affected by the Galactic foreground extinction along the line of sight.

Using the same definition of the extinction spread for all CMDs in Figure 5 allows us to compare to one another the ranges of extinction in the different regions. They are shown in Table 4 for the  $B$ ,  $V$ , and  $I$  bands, respectively indicated as  $\Delta A_B$ ,  $\Delta A_V$ ,  $\Delta A_I$ . The values of  $\Delta A_B$  are directly measured towards NGC 1856 in Figure 5, while those of  $\Delta A_V$  are measured in the same figure along the lines of sight to NGC 1854 and NGC 1858. The extinction law towards 30 Dor West (De Marchi et al. 2014) implies  $A_B = 1.2 A_V$  and this relationship was used here to transform the measured  $\Delta A_B$  values into  $\Delta A_V$ , and viceversa (derived quantities are shown in Italics in Table 4). All values of  $\Delta A_I$  are measured directly for all regions from CMDs similar to those of Figure 5 but in which the  $I$  magnitude is plotted as a function of the  $B-I$  and  $V-I$  colours.

Interestingly, the extinction range appears to increase from Field 1 to Field 4 around NGC 1856 and the growth continues further when moving to NGC 1854 and NGC 1858. A study of the young stellar populations in these fields suggests that there is indeed a correlation between the total amount of extinction and the number of massive stars, as we show in the following.

To allow for a meaningful comparison between these fields, we counted in each of them the number of massive stars with ages between 10 and 40 Myr, which in turn can be interpreted as a proxy for the recent formation of massive stars in these fields. This is achieved by first building the CMDs from all stars present in each field, with no distinction concerning their spatial location. We then drew on the CMDs the isochrones extracted from the models of Chen et al. (2015) for our specific bands and metallicity  $Z = 0.007$  and ages of 10 and 40 Myr, to which we applied the same combination of foreground and intrinsic extinction as in Figure 2 – 4. We finally counted all stars with a MS mass of  $8 M_\odot$  or more, which were identified with the help of the evolutionary tracks. The number of massive objects selected in this way is shown in the last column of Table 4. We note that the number of massive stars measured in this way is necessarily subject to some uncertainty caused by reddening. Some of the stars

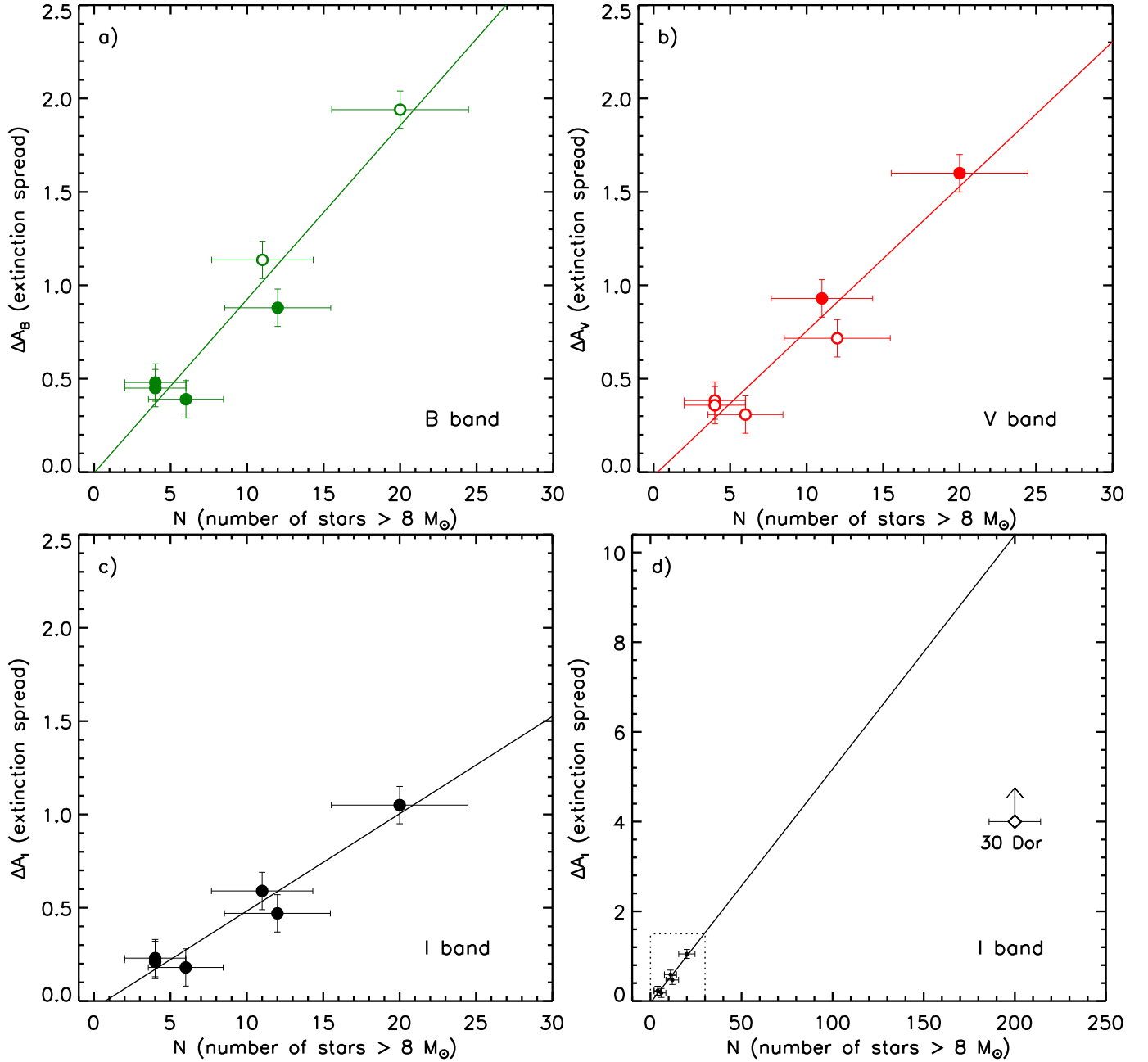


**Figure 6.** Extinction spread in the various regions, as a function of the number of stars more massive than  $8 M_{\odot}$ . Measurements in the  $B$ ,  $V$ , and  $I$  bands are indicated, respectively, in panels a), b), and c). Filled dots mark extinction values measured directly in that band, while empty dots are for measurements derived from neighbouring bands. The lines represent the best linear fit in the three bands. Panel d) is equivalent to panel c), but the range is expanded to accommodate also the data point (lower limit) corresponding to 30 Dor.

redder than the 40 Myr isochrone might in fact be younger objects subject to larger reddening. By the same token, objects younger than 10 Myr might appear redder than the corresponding isochrone. However, we expect the two effects to at least partly compensate, thereby reducing the overall uncertainty.

This analysis reveals that fields containing more massive stars also have typically higher extinction and extinction spread. This is shown graphically in Figure 6. The dots correspond to the values in Table 4 and the green, red, and black colours are used, respectively, for the extinction in the  $B$ ,  $V$ , and  $I$  bands (Panels a, b, and c; panel d, also referring to the  $I$  band data, is discussed further down). The uncertainties in the figure reflect the Poisson statistics on the number of stars

and a typical uncertainty of 0.1 mag on the measured extent of the RC, dictated by the intrinsic RC size mentioned above.

In the  $I$  band we could directly measure  $\Delta A_I$  in all regions (black filled dots). In the  $V$  and  $B$  band, direct measurements are available respectively for NGC 1858 and NGC 1854 (filled red dots), and for fields F1–F4 surrounding NGC 1856 (filled green dots). Empty dots show values obtained from a neighbouring band by interpolation through the extinction law for 30 Dor West (De Marchi et al. 2014), since the latter is fully consistent with the reddening vectors measured in all three clusters in the  $B$ ,  $V$ , and  $I$  bands (see Section 3).

All three sets of  $\Delta A$  values are consistent with simple linear correlations with the number of massive stars, as shown by the solid lines. The formal coefficients are 0.052, 0.077, and

0.093 for the three bands, respectively, with an uncertainty of about 13% ( $1\sigma$ ). Within the uncertainties, we cannot exclude that the best-fitting lines have a zero intercept term. While certainly possible, this does not appear to be likely, because it would imply that the effects of star formation episodes on the local ISM vanish as soon as the last SNe have exploded, contrary to what is observed (e.g., Temim et al. 2015).

What is interesting, however, is not the actual values of the coefficients, which necessarily depend on the selected sample and would be different for another mass range, but rather the existence of a clear correlation between extinction and the number of massive stars in these fields. A linear correlation is also present if the mass range is extended to stars down to  $6M_{\odot}$  and the same age range (10–40 Myr). Further extending the study to less massive stars is not possible without introducing large uncertainties on the age, since the isochrones overlap.

Selecting stars more massive than  $8M_{\odot}$  is relevant because these are the progenitors of core-collapse Type II supernovae (SNe II; e.g. Edlridge & Tout 2004) and we expect objects of this type to be likely at the origin of the anomalous extinction properties that we see in these and other LMC star-forming regions, as suggested by De Marchi & Panagia (2019) and De Marchi et al. (2020). Those works show that the fraction and amount of big grains (with typical size  $\sim 0.1\mu\text{m}$ ) implied by the extinction laws measured in and around 30 Dor and NGC 1938 are quantitatively consistent with the output caused by the SNe II expected to have exploded in those regions in the past  $\sim 50$  Myr. The ejecta from these events appear quantitatively sufficient (De Marchi et al. 2020) to have locally altered the standard grain-size distribution typical of the diffuse ISM of the LMC (e.g., Gordon et al. 2003).

Figure 6 suggests that one can estimate the range of the extinction values in a region of star formation in the LMC by counting the number of massive stars present in that field. The estimate is necessarily approximate, and the relationships shown in Figure 6 are likely to become non linear and to saturate at high extinction values, because highly extinguished RC stars cannot be detected as such.

An example is shown in Figure 6d, where the data from panel 6c (contained within the dotted rectangle) are compared with the data point measured in 30 Dor. To obtain the latter point, we used the photometric catalogue of De Marchi & Panagia (2014), covering the central  $\sim 3 \times 3$  arcmin<sup>2</sup> of 30 Dor, together with the median value of the extinction that they measured towards upper MS stars in that field. We estimate that the central  $\sim 3 \times 3$  arcmin<sup>2</sup> of 30 Dor contain about 200 stars more massive than  $8M_{\odot}$  and with ages between 10 and 40 Myr. The most extinguished RC stars still detectable as such in that field are about 4 mag fainter than the least extinguished ones (see Figure 6 in De Marchi & Panagia 2014). However, objects with even higher extinction (and  $B-V > 2$ ) might well be present in the field, yet they are not detectable because of the limited depth of the observations in the  $B$  band. Therefore, the corresponding data point,  $A_V \simeq 4$  (marked by a diamond in Figure 6d) necessarily represents a lower limit to the maximum extinction value in 30 Dor. That point appears to underestimate by about 60% the amount of extinction that one would obtain by extending the best fitting line in Figure 6c to larger values of  $N$ . Even if there is no guarantee that the relationship that we have measured in our smaller clusters should remain linear in star-forming regions as dense as 30 Dor, the solid line in Figure 6d is likely to provide a re-

alistic estimate of the maximum extinction to be expected in this field, with an uncertainty of less than 50%. In regions of less intense star formation, we expect the uncertainty to be considerably smaller.

In summary, our analysis suggests that it is not the amount of extinction that determines the extinction properties in a region, at variance with what was generally concluded in the 1960s and 1970s from the study of highly extinguished regions of the Galactic Plane (see Introduction). Instead, it appears that recent massive-star formation is systematically accompanied by "non-standard" grey extinction, whose amount is correlated with the star formation strength.

Finally, to characterise the patchiness of the extinction in these regions, we studied the spatial distribution of highly extinguished RC stars. We show an example in Figure 7 for the case of the region around NGC 1858. We took as candidate RC stars all objects in the CMD contained within  $\pm 0.4$  mag of the reddening vector shown in Figure 5a and fainter than  $V = 19$ . A total of 582 stars satisfy this condition: although some of them might in fact be RGB stars, we expect the majority to be RC objects. About 80 % of them have extinction  $A_V < 1.0$  and the remaining 20 % have values in the range  $1.0 < A_V < 1.5$ . We compare the positions and spatial distributions of these two groups in Figure 7a by means of lines of stellar density with constant logarithmic steps set at 2, 4, and 8 times the mean density of each group. The contour plots were obtained after smoothing the actual distribution with a Gaussian beam with  $\sigma = 2''$ , as indicated by the circle at the top of the figures. The grey shaded contours correspond to the low-reddening RC stars and the red contour lines to highly reddened RC objects. Figure 7a reveals that the low-reddening RC stars are more uniformly distributed than the RC objects with higher extinction. In Figure 7b we compare, using the same relative contour levels, the distribution of the highly reddened RC stars (red contour lines; same as in panel a) with that of the massive MS stars ( $> 8M_{\odot}$ ; blue shaded contours). Although qualitative, this comparison shows that the distribution of the highly reddened RC stars is rather similar to that of the massive stars. This suggests that a considerable fraction of the absorbing material along the lines of sight to these RC stars is indeed associated with the region of recent star formation.

## 6. CONCLUSIONS

We conclude with some considerations on the nature of the relationships highlighted in Figure 6, which is not completely unexpected. The typical dust extinction of star-forming galaxies is known to increase with their total stellar mass  $M_*$ , not only in the local universe but also out to redshift of at least  $z \simeq 2$  (e.g., Brinchmann et al. 2004; Stasinska et al. 2004; Pannella et al. 2009). In the range  $10^8 \lesssim M_*/M_{\odot} \lesssim 10^{10}$ , the extinction has been shown to increase monotonically and approximately linearly with  $\log M_*$  (Garn & Best 2010; Zahid et al. 2013). Also the rate of star formation and the metallicity of these galaxies correlate with the extinction, but the predominant factor influencing it appears to be the stellar mass (Garn & Best 2010).

To be sure, the total mass of the star-forming regions probed by our study is some  $\sim 4$  orders of magnitude smaller than that of the smallest of the high-redshift star-forming galaxies mentioned above. As an example, adopting for NGC 1854 a standard initial mass function (e.g. Kroupa 2001) with a power-law index  $\gamma = -2.3$  for stars more massive than  $0.5M_{\odot}$  and  $\gamma = -1.3$  in the  $0.08 - 0.5M_{\odot}$  range, we derived

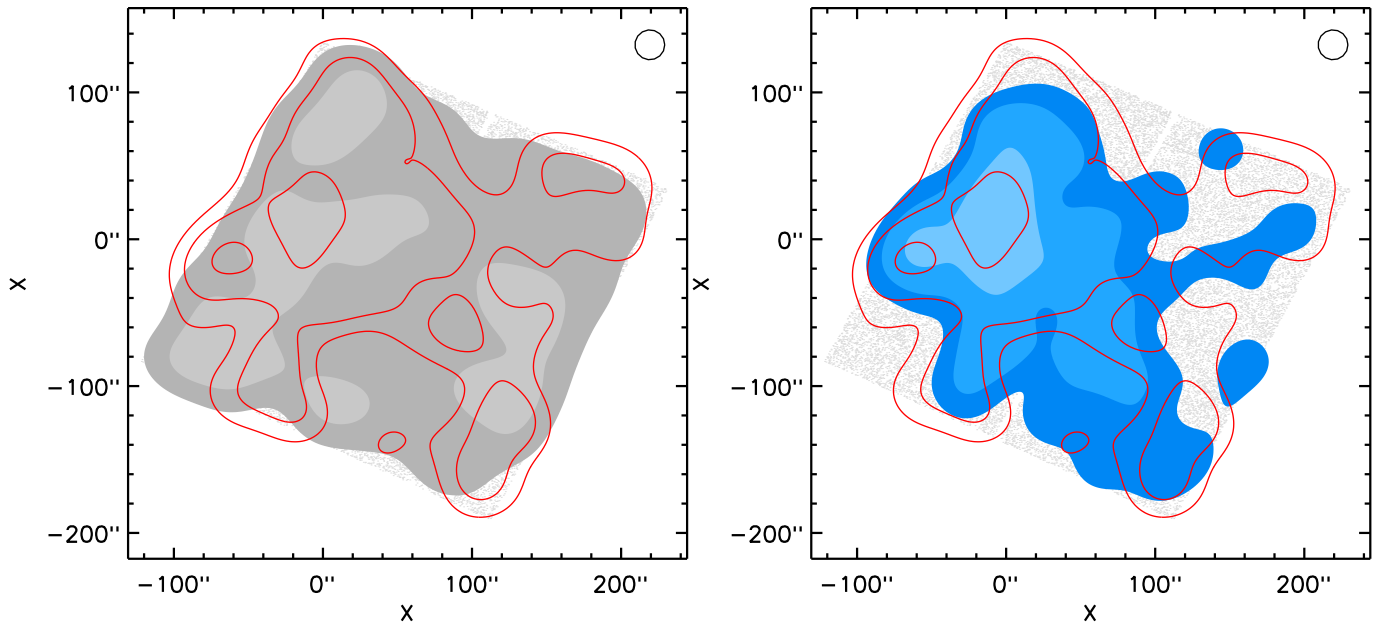


**Figure 7.** Contour plots showing the position and density distribution of RC and upper MS stars in the field containing NGC 1858. The coordinates system is centred on the nominal cluster centre. Red contour lines are used for highly reddened RC stars ( $A_V > 1$ ), while the grey and blue shadings are used for low-reddening RC stars and upper MS objects, respectively. The lower contour level corresponds to twice the mean density of each group. The circles at the top of the panels show the size of the Gaussian beam used for smoothing the actual distributions.

a total initial mass of about  $2.5 \times 10^4 M_\odot$  for this cluster. Nonetheless, the stars responsible for the bulk of the dust, and particularly of the big grains that we detect in our regions, are massive stars of the same type as those whose emission line fluxes are used to infer both the total extinction and  $M_*$  values of the star-forming galaxies. These are the objects more massive than  $8 M_\odot$  that end their lives as SNe II (e.g. Dwek 1998).

Although so far limited in size, our sample is potentially better suited to studying the actual physical mechanisms at the origin of the observed correlations. In our sample, the total mass, i.e. the number of stars, is measured directly by counting individual objects, so we do not have to rely on necessarily uncertain integrated quantities often derived through approximate model-based relations (e.g. Kauffmann et al. 2003): instead, we have direct measurements. Also the extinction properties (and extinction law) are directly measured by us in our fields, including the value of  $R_V$ . Other studies instead assume an average value of  $R_V$ , which is known to be affected by large uncertainties (Calzetti et al. 2000) and is not applicable outside the regime of centrally-concentrated starburst galaxies

(Calzetti et al. 2021). Furthermore, the fact that the empirical relationships that we discovered from a limited number of small star-forming regions is able to reproduce, to within a factor of two, also to the case of 30 Dor suggests that these relationships are meaningful also for the intense star-forming knots of high-redshift galaxies that 30 Dor mimics (e.g., Doran et al. 2013; Crowther et al. 2017). Extending our study of the extinction properties to a number of other star-forming regions in the LMC (De Marchi et al., in prep) will allow us to better constrain the nature of the physical processes at play.

We are very grateful to an anonymous referee whose expert advice and constructive criticism have helped us to improve the presentation of this work. APM acknowledges support from the European Research Council (ERC) under the European Union's Horizon 2020 research innovation programme (Grant Agreement ERC-StG 2016, No 716082 'GALFOR', <http://progetti.dfa.unipd.it/GALFOR>), by the MIUR through the FARE project R164RM93XW 'SEMPLICE' and the PRIN programme 2017Z2HSMF.

## REFERENCES

- Alcaino, G., Liller, W. 1987, *AJ*, 94, 372  
 Andersen, M., Gennaro, M., Brandner, W., et al. 2017, *A&A*, 602, A22  
 Anderson, J., King, I. 2006, Instrument Science Report ACS 2006-01, (Baltimore: STScI)  
 Anderson, J., Sarajedini, A., Bedin, et al. 2008, *AJ*, 135, 2055  
 Bastian, N., Silva-Villa, E. 2013, *MNRAS*, 431, L122  
 Bonanos, A., Massa, D., Sewilo, M., et al. 2009, *AJ*, 138, 1003  
 Brinchmann, J., Charlot, S., White, S., et al. 2004, *MNRAS*, 351, 1151  
 Calzetti, D., Armus, L., Bohlin, R., et al. 2000, *ApJ*, 533, 682  
 Calzetti, D., Battisti, A., Shivaee, I., et al. 2021, *ApJ*, 913, 37  
 Caplan, J., Deharveng, L. 1984, in "Structure and Evolution of the Magellanic Clouds", IAU Symposium 108, Ed. S. van den Bergh, K. de Boer (Dordrecht: D. Reidel), 389  
 Connolly, L., Tift, W. 1977, *MNRAS*, 180, 401  
 Crowther, P., Castro, N., Evans, C., et al. 2017, *Msngr*, 170, 40  
 Cardelli, J., Clayton, G., Mathis, J. 1989, *ApJ*, 345, 245  
 Chen, Y., Bressan, A., Girardi, L., et al. 2015, *MNRAS*, 452, 1068  
 Correnti, M., Goudfrooij, P., Puzia, T., de Mink, S. 2015, *MNRAS*, 450, 3054  
 D'Antona, F., Di Criscienzo, M., Decressin, T., et al. 2015, *MNRAS*, 453, 2637  
 De Marchi, G., Panagia, N. 2014, *MNRAS*, 445, 93  
 De Marchi, G., Panagia, N. 2019, *ApJ*, 878, 31  
 De Marchi, G., Panagia, N., Girardi, L. 2014, *MNRAS*, 438, 513  
 De Marchi, G., Panagia, N., Milone, A. 2020, *ApJ*, 899, 114  
 De Marchi, G., Panagia, N., Sabbi, E., et al. 2016, *MNRAS*, 455, 4373  
 Doran, E., Crowther, P., de Koter, A., et al. 2013, *A&A*, 558, A134  
 Eldridge, J., Tout, C. 2004, *MNRAS*, 353, 87  
 Epchtein, N., Braz, M., Sevre, F. 1984, *A&A*, 140, 67  
 Fitzpatrick, E., Massa, D. 2005, *AJ*, 130, 1127  
 Fitzpatrick, E., Savage, B. 1984, *ApJ*, 279, 578  
 Garn, T., Best, P. 2010, *MNRAS*, 409, 421  
 Gilliland, R. 2004, Instrument Science Report ACS 2004-01, (Baltimore: STScI)  
 Geha, M., Holtzman, J., Mould, J., et al. 1998, *AJ*, 115, 1045  
 Girardi L., Salaris M., 2001, *MNRAS*, 323, 109

- Gordon, K., Clayton, G., Misselt, K., Landolt, A., Wolff, M. 2003, *ApJ*, 594, 279
- Herbst, W. 1975, *AJ*, 80, 492
- Hill, V., Andrievsky, S., Spite, M. 1995, *A&A*, 293, 347
- Hodge, P., 1983, *ApJ*, 264, 470
- Kauffmann, G., Heckman, T., White, S., et al. 2003, *MNRAS*, 341, 33
- Kroupa, P. 2001, *MNRAS*, 322, 231
- Massa, D., Savage, B., Fitzpatrick, E. 1983, *ApJ*, 266, 662
- Milone, A., Bedin, L., Piotto, G., et al. 2015, *MNRAS*, 450, 3750
- Milone, A., Stetson, P., Piotto, G., et al. 2009, *A&A*, 503, 755
- Nataf, D. M., Gould, A., Fouqué, P., et al. 2013, *ApJ*, 769, 88
- Panagia N. 1998, *Mem. Soc. Astron. Ital.*, 69, 225
- Panagia N. 1999, in Chu Y.-H., Suntzeff N., Hesser J., Bohlender D., eds, *Proc. IAU Symp. 190, New Views of the Magellanic Clouds* (San Francisco: Astron. Soc. Pac.), 549
- Panagia N., Gilmozzi R., Macchetto F., Adorf H.-M., Kirshner R., 1991, *ApJ*, 380, L23
- Pannella, M., Carilli, C., Daddi, E., et al. 2009, *ApJL*, 698, L116
- Ryon, J. 2019, *ACS Instrument Handbook*, Version 19 (Baltimore: STScI), <https://hst-docs.stsci.edu/acsihb>
- Salaris M., Girardi L., 2002, *MNRAS*, 337, 332
- Sharpless, S. 1952, *AJ*, 116, 251
- Sharpless, S. 1962, *ApJ*, 136, 767
- Stasińska, G., Mateus, A., Sodré, L., Szczerba, R. 2004, *A&A*, 420, 475
- Tang, J., Bressan, A., Rosenfield, P., et al. 2014, *MNRAS*, 445, 4287
- Temim, T., Dwek, E., Tchernyshyov, K., et al. 2015, *ApJ*, 799, 158
- Turner, D. 1973, *AJ*, 78, 597
- Vallenari, A., Aparicio, A., Fagotto, F., et al. 1994, *A&A* 284, 447
- van der Marel, R., Cioni, M. 2001, *AJ*, 122, 1807
- Zahid, H., Yates, R., Kewley, L., Kudritzki, R. 2013, *ApJ*, 763, 92